PAPER

Check for updates

Molecular insights into competitive adsorption of CO_2/CH_4 mixture in shale nanopores

Wenning Zhou, [ID] *[ab] Zhe Zhang,[a] Haobo Wang,[a] Yuying Yan[c] and Xunliang Liu[ab]

In the present study, competitive adsorption behaviour of supercritical carbon dioxide and methane binary mixture in shale organic nanopores was investigated by using grand canonical Monte Carlo (GCMC) simulations. The model was firstly validated by comparing with experimental data and a satisfactory agreement was obtained. Then the effects of temperature (298–388 K), pressure (up to 60 MPa), pore size (1–4 nm) and moisture content (0–2.4 wt%) on competitive adsorption behaviour of the binary mixture were examined and discussed in depth. It is found that the adsorption capacity of carbon dioxide in shale organic nanopores is much higher than that of methane under various conditions. The mechanism of competitive adsorption was discussed in detail. In addition, the results show that a lower temperature is favorable to both the adsorption amount and selectivity of CO_2/CH_4 binary mixture in shale organic nanopores. However, an appropriate CO_2 injection pressure should be considered to take into account the CO_2 sequestration amount and the exploitation efficiency of shale gas. As for moisture content, different influences on CO_2/CH_4 adsorption selectivity have been observed at low and high moisture conditions. Therefore, different simulation technologies for shale gas production and CO_2 sequestration should be applied depending on the actual moisture conditions of the shale reservoirs. It is expected that the findings in this work could be helpful to estimate and enhance shale gas resource recovery and also evaluate CO_2 sequestration efficiency in shale reservoirs.

Introduction

With the increasing global demand for energy, there is a growing interest in unconventional oil and gas resources. Shale gas, as a clean and efficient unconventional gas resource, has become an important alternative to conventional fossil energy. Over the last decade, shale gas has been successfully recovered due to the development of horizontal drilling and massive hydraulic fracturing technology and recently extensively explored in the US, Canada, Australia, Europe, China, *etc.*[1,2] However, hydraulic fracturing has a few drawbacks, including potential surface water shortage due to high-volume hydraulic fracturing, risks of ground and surface water contamination caused by additives in the fracturing fluid, the accumulation of toxic and radioactive elements in soil, risk of induced seismicity by large-scale wastewater disposal, *etc.*[3–5] Therefore, seeking an alternative fracturing fluid has received considerable attention from researchers. Meanwhile, carbon emission has been another hot topic due

to the fact of global warming. Carbon capture, utilization and storage (CCUS) has been proposed as the most attractive and promising technology to reduce carbon emission and thereby mitigate global warming.[6–8] Among various carbon utilization and storage techniques, the most promising systems are depleted oil reservoirs, particularly those suited to CO_2-based Enhanced Oil/Gas Recovery (EOR/EGR), and deep saline formations.[9]

Carbon dioxide enhanced shale gas recovery has recently drawn more and more attention. Shale gas is mainly composed of free gas in fractures and pores, adsorbed gas in organic matter and clay minerals and a small amount of dissolved gas in liquid phase. Of the three forms above, the adsorbed gas takes up 20–85% of the total gas-in-place. The percentage could account for 60–85% in the organic-rich shale.[10] Due to the characteristics of supercritical carbon dioxide (Sc-CO_2), including its low viscosity, high diffusion capacity near gas and high density near liquid, it has unique advantages for the shale gas extraction.[11] Additionally, much research has shown that preferential adsorption of carbon dioxide over methane, which indicates the feasibility of CO_2 sequestration with enhanced gas recovery (CS-EGR) in shale reservoirs.[12,13] Although the CS-EGR technique in shale has not yet been widely commercialized, extensive investigations have been carried out in this field.[14–16] Weniger *et al.*[17] conducted experiments of high-pressure methane and carbon dioxide sorption

[a]School of Energy and Environmental Engineering, University of Science and Technology Beijing, Beijing 100083, China. E-mail: wenningzhou@ustb.edu.cn; Tel: +86 10 62332730

[b]Beijing Key Laboratory of Energy Saving and Emission Reduction for Metallurgical Industry, University of Science and Technology Beijing, Beijing 100083, China

[c]Fluids & Thermal Engineering Research Group, Faculty of Engineering, University of Nottingham, Nottingham NG7 2RD, UK

on shale examples. They reported that the CO_2 and CH_4 sorption capacities correlated with the organic carbon content (TOC) and CO_2/CH_4 sorption capacity ratio ranged between 1.9 and 6.9 for carbonaceous shale. Duan et al.[18] experimentally examined the adsorption equilibrium isotherms of CH_4, CO_2 and their mixtures on Sichuan Basin shale, China. Their results clearly indicated that adsorbed CO_2 is in a more highly ordered arrangement than CH_4 on shale and their selectivity depends upon the composition and pore structure of the shale. In addition, a series of experiments have been carried out to investigate carbon dioxide and methane adsorption capacity on the shale and discuss the influences of pressure, temperature, pore structure and moisture content.[19–22] More recently, researchers also performed fracturing experiments on shale samples using Sc-CO_2 and water.[23,24] Their results demonstrated Sc-CO_2 fracturing has absolute advantages over hydraulic fracturing in the fracture initiation pressure and creating more extensive fracture network, thereby increasing the permeability and promoting gas transport. Although much experimental work has been done, it is difficult to reveal the essence of CO_2/CH_4 competitive adsorption behaviours through laboratory experiments due to the complexity of the shale structure and associated geological conditions.

In recent years, molecular simulation has emerged as an effective approach in addition to experimental and theoretical methods to study the microscopic molecular interaction mechanism.[25] Supercritical methane diffusion behaviour in the slit-shaped nanopores in shale was investigated by molecular simulation in the work.[26] Their results showed that methane molecules in shale nanopores diffuse more rapidly with the increasing pore size and temperature but diffuse more slowly with an increase in pressure. Liu et al.[27] carried out molecular dynamics simulations to study the competitive adsorption and diffusion performances of CO_2/CH_4 binary mixture within shale organic nanochannels. They found preferential adsorption of CO_2 over CH_4 on the nanochannel surface and CO_2/CH_4 selectivity and mobility are affected by temperature. Zhang et al.[28] used molecular simulation to explore the adsorption and CO_2/CH_4 selectivity in functional group rich shale nanopores. They reported the functional group rich organic matter in shale has a significant effect on the selectivity of CO_2/CH_4 and suggested an optimum depth for CO_2 sequestration. Pathak et al.[29] employed molecular simulations to investigate CO_2/CH_4 adsorption performance on kerogen in organic rich shale matrix. The results revealed that the carbon dioxide is more strongly retained than methane in the bulk kerogen matrix. Lin et al.[30] and Yu et al.[31] examined methane adsorption and diffusion behaviours in slit-shaped shale organic nanopores represented by graphene. The adsorption properties of in quartz clay minerals of shale matrix were also studied by employing molecular simulations.[32,33] Moreover, the effects of moisture content on adsorption of methane adsorption and diffusion in kerogen and kaolinite were explored by molecular simulations.[26,34,35] Their results indicated that moisture content has a great influence on methane adsorption and diffusion behaviours in shale. Although much work has been carried out on studying

shale gas adsorption and diffusion mechanisms, only a few of them focus on CO_2/CH_4 mixture and the mechanism of competitive adsorption in organic shale nanopore has not been fully understood. In this study, molecular simulation was adopted to investigate CO_2/CH_4 binary mixture competitive adsorption behaviours in slit nanopores of shale organic matter. Effects of temperature, pressure, pore size and moisture content on CO_2/CH_4 binary mixture competitive adsorption performances were investigated and discussed in depth. The results are expected to serve as a reference for the enhancement of shale gas exploitation and evaluation of CO_2 sequestration capacity in shale matrix.

Models and methods

Model construction

The constituents of shale matrix include organic matter and inorganic substances, with large amount of shale gas mainly absorbing on organic matter. The nanopores in shale gas reservoirs are mainly organic matter nanopores. When the adsorption and desorption properties of shale gas are concerned, graphene slit-shaped nanochannel were widely employed as a representation of organic matter nanopore and showed satisfactory results.[25–27,29,30] In this study, a multilayer graphene slit was built up to investigate CO_2/CH_4 binary mixture competitive adsorption characteristics, as shown in Fig. 1. This periodic, optimized, slit-shaped nanochannel consists of upper and lower three-layer graphene with the interlayer spacing of 0.335 nm.[36] The distance between upper and lower grapheme layer, i.e., size of shale organic nanopores, ranges from 1 nm to 4 nm.

Molecular simulation

In the present study, the grand canonical Monte Carlo (GCMC) method was employed and all simulations were performed with Accelrys Materials Studio software. The COMPASS force field was adopted in the simulations. Simulation cases were carried out with 1×10^7 Monte Carlo steps.[37,38] The first 5×10^6 steps were performed to guarantee the equilibrium state. The latter 5×10^6 steps were used for the ensemble averages to calculate the required physical parameters. Moreover, we used the Ewald method to describe the electrostatic interactions with the accuracy of 10^{-3} kcal mol^{-1}. The van der Waals (vdW) interactions were calculated within a fine cutoff distance of 15.5 Å by
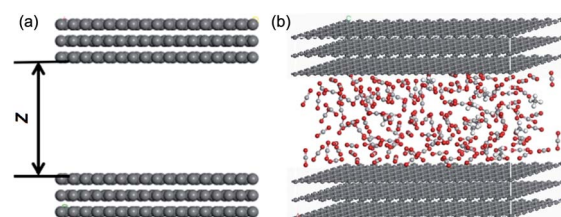

Fig. 1 Graphene slit model for the organic nanopore in shale: (a) 2D; (b) 3D vision with adsorbed CO_2/CH_4 binary mixture.

Paper

the atom-based method. Interactions between organic matter and gas molecules were described using the Lennard-Jones (LJ) 12-6 potential:

$$U_{LJ}(r_{ij}) = \begin{cases} 4\varepsilon_{ij}\left[\left(\dfrac{\sigma_{ij}}{r_{ij}}\right)^{12} - \left(\dfrac{\sigma_{ij}}{r_{ij}}\right)^{6}\right] & (r_{ij} \leq r_{cut}) \\ 0 & (r_{ij} > r_{cut}) \end{cases} \quad (1)$$

where r_{ij} is the separation of the pair of atoms i and j, r_{cut} is the cutoff distance in the L-J potential, ε is the depth of the potential well and σ is the finite distance at which the inter-particle potential is zero. The Lorentz–Berthelot classical mixing rule was used to calculate the parameters for unlike atoms in the L-J potential:

$$\sigma_{ij} = \frac{1}{2}(\sigma_{ii} + \sigma_{jj}) \quad (2)$$

$$\varepsilon_{ij} = \sqrt{\varepsilon_{ii}\varepsilon_{jj}} \quad (3)$$

It should be mentioned that in the GCMC simulation, chemical potential, volume and temperature are independent variables. The chemical potential is a function of fugacity rather than pressure. Therefore, the Peng–Robinson (P–R) equation of state was used to calculate the fugacity of CH_4 and CO_2 mixture in this study.[39] The adsorption amount obtained in simulations is the absolute amount. To compare with the adsorption amount in experiments, where excess amount is used, the following expression is applied:

$$n^{ex} = n^{abs} - \rho^{b}V_{ads} \quad (4)$$

where n^{ex} and n^{abs} are the excess and absolute amounts adsorbed, respectively. ρ^{b} is the density of the bulk phase at the conditions of interest, calculated using the P–R equation of state. V_{ads} is the pore volume.

To examine the competitive adsorption behaviours, the adsorption selectivity of CO_2 over CH_4 is defined:

$$S_{CO_2/CH_4} = \frac{x_{CO_2}/x_{CH_4}}{y_{CO_2}/y_{CH_4}} \quad (5)$$

where x_i denotes the mole fraction of component i in the adsorption phase, while y_i is the mole fraction of component i in the bulk phase. It indicates that the preferential adsorption of CO_2 is greater than that of CH_4 to shale organic nanopore when the adsorption selectivity $S_{CO_2/CH_4} > 1$. A higher selectivity indicates a stronger adsorption capacity of CO_2 over CH_4.

To study the effects of water content on absorption, we used the average water density to quantify the moisture content:

$$\rho_{H_2O}^{ave} = \frac{N_{H_2O}M_{H_2O}}{V\varpi N_A} \quad (6)$$

where N_{H_2O} is the number of H_2O molecules, M_{H_2O} is the water molar weight, V is the volume of the slit nanopore, N_A is Avogadro's number and ϖ is the moisture.

Results and discussion

Model validation

To validate the proposed model, simulation results of CH_4 adsorption isotherms were compared with experimental results[40] and Langmuir single-molecular layer adsorption theory,[41] which is widely applied to describe gas adsorption in shale matrix, as shown in Fig. 2. It should be mentioned that the excess adsorption capacity has been converted to absolute adsorption capacity to compare with the simulation results obtained by the GCMC. The simulation was performed in a pressure range of 1.25–20 MPa at the temperature of 333.15 K, which are the same conditions with those in experimental work. It is found that simulation results fit very well with Langmuir equation and also show satisfactory agreement with experimental data. It should be noted that, besides temperature and pressure, the adsorption capacity of CH_4 in actual shale organic matter relates with many other factors such as the total carbon content (TOC), organic matter type and maturity, pore structure, moisture, etc.[38,42] The simulation result in the present study was obtained at the pore size of 1.5 nm shale organic nanopore in dry condition. Nevertheless, the agreement in the tendency and data of the comparison has proved the GCMC as an effective and valid tool to explore the adsorption characteristics of the gases at microscopic scale in shale matrix. Therefore, the validity of the model is justified and further investigation on CO_2/CH_4 binary mixture adsorption can be then carried out.

Effects of temperature on competitive adsorption isotherms

In actual shale formations, the reservoir depth varies from 1000 m to 4000 m. According to the geothermal gradient of ~3 °C/100 m, the temperatures of shale formations would be different depending on their depths. In this study, a wide temperature range of 298 K to 388 K was examined. The effects of temperature on CH_4, CO_2 and CO_2/CH_4 binary mixture adsorption behaviours were investigated. Fig. 3 and 4 display the effects of temperature on adsorption isotherms for CH_4 and CO_2, respectively.
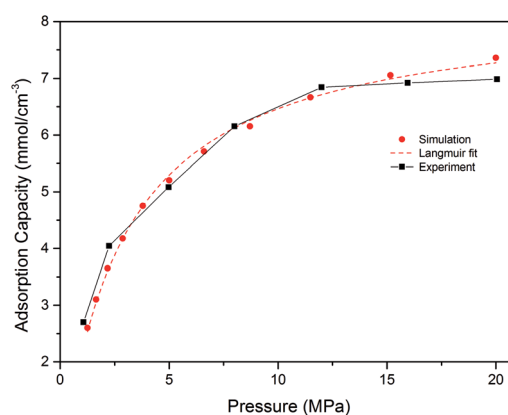

Fig. 2 Comparison of adsorption isotherms from simulation and experiment at 333.15 K.
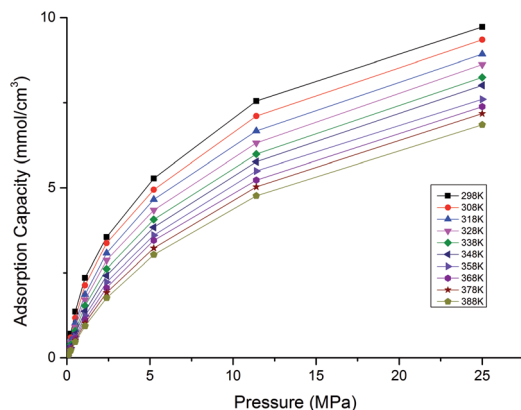
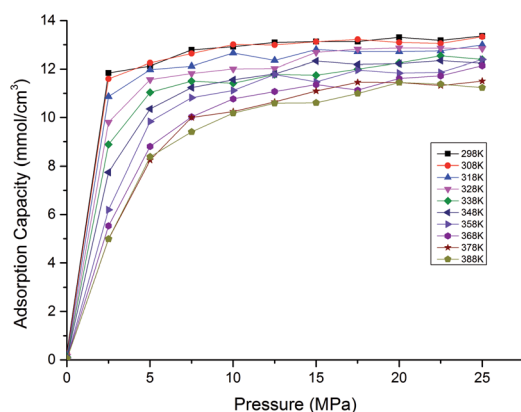**Fig. 3** Adsorption isotherms of CH_4 at different temperatures.

Fig. 4 Adsorption isotherms of CO_2 at different temperatures.

The results show that for both CH_4 and CO_2, the adsorption capacities decrease with the increasing temperature. It is because that CH_4 and CO_2 adsorption in shale organic matter is physical adsorption.[19,20] The increasing temperature leads to increases of the mean kinetic energy of CH_4 and CO_2 gas molecules, which would enable them to conquer and escape from the adsorption layer easier. It can be also observed from the figures that CO_2 is adsorbed much faster into shale organic matter than CH_4 as the pressure increases.

Fig. 5 presents the effects of temperature on the competitive adsorption behaviour of CO_2/CH_4 binary mixture in shale organic nanopore. It is found that, under the same temperature and pressure condition, the adsorption capacity of CO_2 is far greater than that of CH_4. The reasons might be as follows. As the adsorption of CO_2/CH_4 on shale organic matter is physical adsorption, the adsorption strength is mainly determined by adsorbent–adsorbate interaction energy. Compared with CH_4 molecules, the large quadrupole moment of CO_2 results in strong Coulomb interaction between CO_2 and the surfaces of the nanopore.[43] So both Coulomb interaction and van der Waals interaction, which is determined by the polarizability, contribute the interactions between CO_2 and shale organic matter, with the Coulomb interaction being much stronger. While CH_4 is a nonpolar molecule, the van der Waals force is
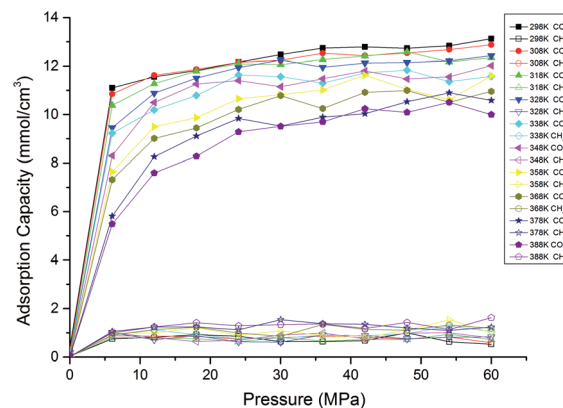

Fig. 5 Competitive adsorption isotherms of CO_2/CH_4 in shale organic nanopore at different temperatures.

Table 1 Properties of CO_2 and CH_4

Properties	CO_2	CH_4
Molecular weight (g mol^{-1})	44	16
Kinetic diameter (Å)	3.3	3.8
Polarizability $\times 10^{25}$ cm^3	26.3	26.0
Quadrupole moment $\times 10^{26}$ esu cm^2	4.3	0
Dipole moment $\times 10^{18}$ esu cm	0	0

the only interaction between CH_4 and shale organic nanopore. The properties of the adsorbates CO_2 and CH_4 can be seen in Table 1. Besides adsorbent–adsorbate interaction, adsorbate–adsorbate interaction also contributes the adsorption strength.[44] On the one hand, the critical temperature for CO_2 is 31.1 °C, which is higher than that for CH_4 (-82.6 °C). Thus it is relatively easy for CO_2 gas to be liquefied. The stronger attraction between CO_2 molecules makes them much easier to be adsorbed by shale organic matter. On the other hand, larger dynamic viscosity of CH_4 under shale reservoirs conditions results in more intense and irregular thermal motion of CH_4 molecules, causing higher desorption ability of CH_4 from the shale organic matter. Therefore, the interactions between CO_2 and shale organic nanopore are much stronger than that between CH_4 and the nanopore. It can be seen from Fig. 5, at the pressure of 20 MPa and temperature of 298 K, the competitive adsorption capacity of CH_4 is only around 1 mmol cm^{-3}, while the adsorption capacity of CO_2 is as high as 12 mmol cm^{-3}. The adsorption capacity of CH_4 single component is around 7.5 mmol cm^{-3} according to the data in Fig. 3. That is to say, the adsorption capacity of CH_4 is largely suppressed under competitive conditions with CO_2 in shale organic matter. In another word, CO_2 is preferentially adsorbed over CH_4 in organic nanopore in shale. Similar results have been reported in previous experimental works.[18,20,45]

Fig. 6 plots the adsorption selectivity of CO_2/CH_4 binary mixture in shale organic nanopore as a function of temperature at different CO_2 injection pressures. It shows that the temperature has great influence on the selectivity of CO_2/CH_4, *i.e.*, the
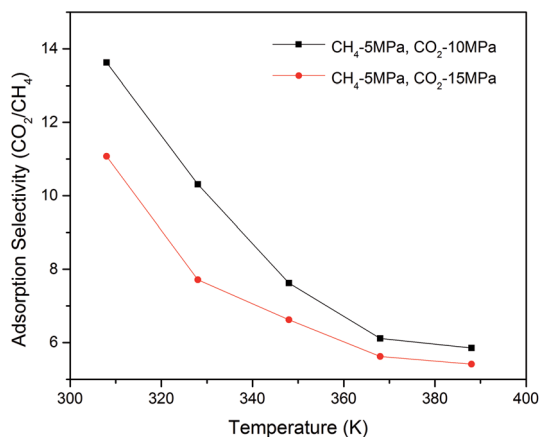
Fig. 6 Adsorption selectivity of CO_2/CH_4 in shale organic nanopore as a function of temperature at different pressures.
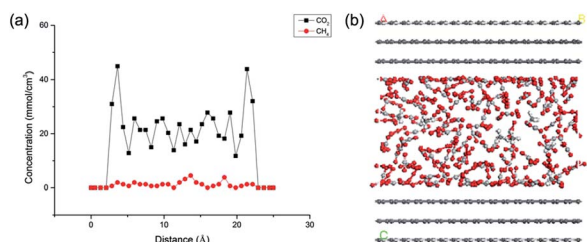

Fig. 7 Concentration profile (a) and snapshot (b) of CO_2/CH_4 binary mixture adsorption in the slit-like nanopore of shale organic matter.

CO_2 sequestration efficiency. A lower temperature is favourable to the enhancement of selectivity. As the temperature goes up, the selectivity decreases significantly. At the same partial pressure of CH_4, a lower CO_2 injection pressure would be also helpful to the increase of the selectivity.

Effects of pressure on competitive adsorption behaviours

To reveal the effects of pressure on CO_2/CH_4 competitive adsorption characteristics, a series of simulation cases were conducted. The pressure conditions as a function of depth can be estimated by the pressure gradient ∼1.0 MPa/100 m. Indeed, the pressure change of shale gas is complicated and exhibits a tendency of decline as the exploitation progresses. Thus a wide range of CH_4 partial pressure 5–20 MPa and CO_2 injection pressure 7–30 MPa was applied in the simulations. Fig. 7(a) illustrates the concentration profile of CO_2/CH_4 binary mixture in the nanopore of shale organic matter at the temperature of 308 K with the CO_2 injection pressure of 10 MPa and CH_4 partial pressure of 5 MPa. It is found that, when together with carbon dioxide, the adsorption amount of CH_4 on shale organic matter decreases significantly. The snapshot of the adsorption is shown in Fig. 7(b).

Fig. 8 presents the adsorption amount of CO_2/CH_4 binary mixture as a function of CO_2 injection pressure at different CH_4 partial pressures. It is observed that with the increasing CO_2 injection pressure, the adsorption amount of CO_2 has a gradual
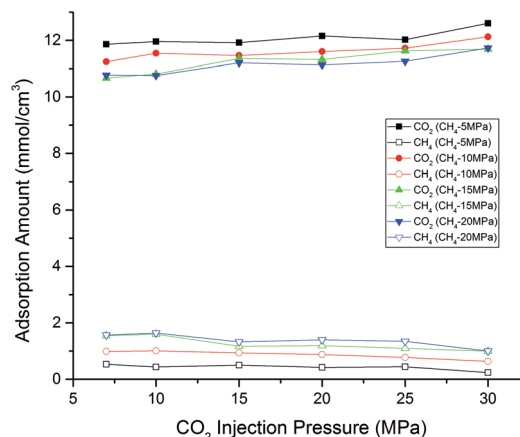

Fig. 8 Adsorption amount of CO_2/CH_4 binary mixture as a function of CO_2 injection pressure at different CH_4 partial pressures.

rise while the trend has a decline for CH_4. However, the increasing CO_2 injection pressure also leads to the decrease of CO_2/CH_4 adsorption selectivity, as shown in Fig. 6. Therefore, an appropriate CO_2 injection pressure should be chosen to take into account CO_2 sequestration amount and CO_2/CH_4 adsorption selectivity in CS-EGR project. In addition, it can be seen from the figure as the partial pressure of CH_4 goes up, the differences between CO_2 and CH_4 adsorption capacity become smaller. In another word, the efficiency of CO_2 sequestration and enhancement recovery of shale gas would have a gradual decline as the pressure (i.e., the depth of shale formations) increases.

Effects of pore size on competitive adsorption behaviours

Due to the fact that a large proportion of pores in shale matrix are nanosized, it is essential to examine the influences of pore size on the competitive adsorption behaviours of CO_2/CH_4 binary mixture. Fig. 9 shows the snapshots of CO_2/CH_4 binary mixture adsorption for nanopores with the pore size ranging from 1 nm to 2.5 nm.

Fig. 10 displays the competitive adsorption isotherms of CO_2/CH_4 in shale nanopores with different pore sizes from 1 nm to 4 nm at the temperature of 318 K. It is found that, under a wide range of pressure, the adsorption amount for CO_2 increases significantly when the pore size increase from 1 nm to 2.5 nm. However, when the pore size further increases, the increase of CO_2 adsorption amount becomes more gradual.

Fig. 11 shows the adsorption selectivity of CO_2/CH_4 as a function of pore size at the temperature of 318 K. It can be seen that the selectivity increases at the beginning stage when the pore size is extremely small (∼1 nm). This is because the pore size of 1 nm is comparative the size of CH_4 and CO_2 molecule, the kinetic diameters of which are 3.8 Å and 3.3 Å, respectively. The very small adsorption amount leads to a relatively small selectivity. However, a further increase of the pore size leads to a decline of the selectivity. The optimum selectivity occurs at the pore size of 1.5–2 nm. It can be seen from the figure, all selectivities of the studied cases in the present work
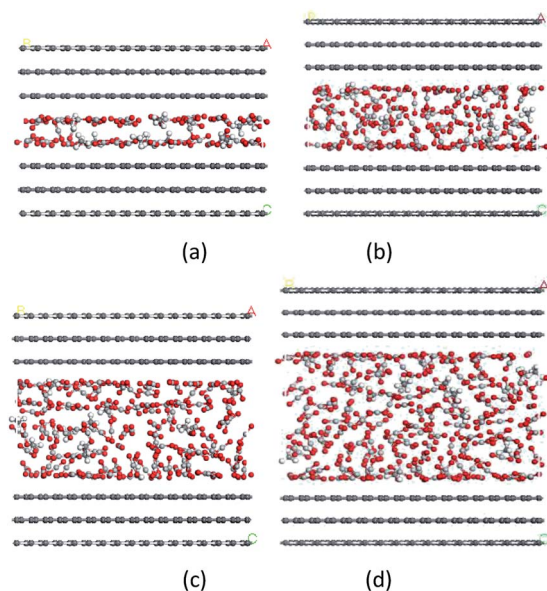
Fig. 9 Snapshots of CO_2/CH_4 binary mixture adsorption for nanopores with different pore sizes: (a) 1 nm; (b) 1.5 nm; (c) 2 nm; (d) 2.5 nm.
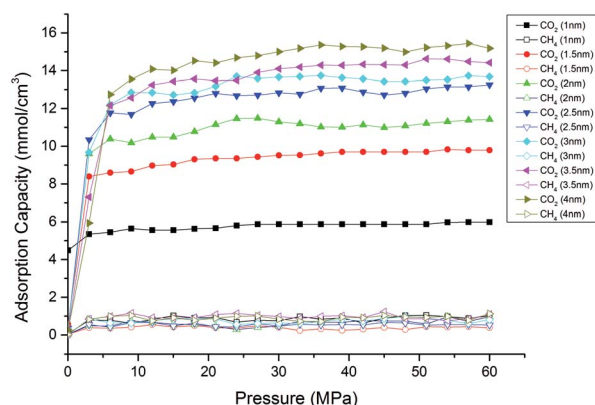

Fig. 10 Competitive adsorption isotherms of CO_2/CH_4 in shale organic nanopores with different pore sizes.

are larger than 6 for the nanopores ranging from 1.5 nm to 4 nm in pore size. In addition, the result shows that the selectivity decreases as the increasing CO_2 injection pressures. These findings indicate that carbon dioxide is suitable for enhancing shale gas recovery with the CO_2 sequestration.

Effects of moisture content on competitive adsorption behaviours

In this section, the effects of moisture content on CO_2/CH_4 mixture adsorption performances were explored. A certain number of H_2O molecules, which was determined by eqn (5), were pre-loaded in shale nanopore to achieve the desired moisture content. The concentration profile of CO_2/CH_4 mixture in the nanopore at the temperature of 318 K with different moisture contents is shown in Fig. 12. It is observed that the peak concentration for CO_2 near the pore wall declines
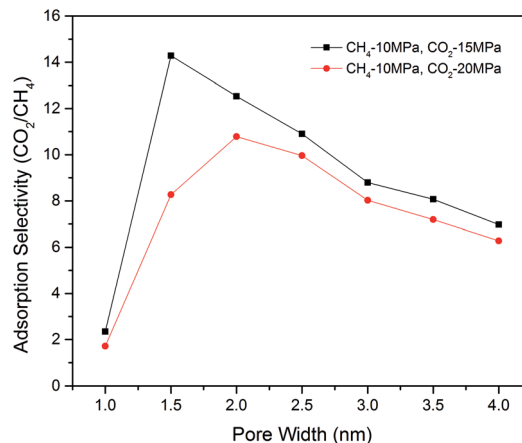

Fig. 11 Adsorption selectivity of CO_2/CH_4 in shale organic nanopore as a function of pore size at different pressures.

with the increasing moisture content. The effect of moisture content on CH_4 is less significant. Fig. 13 demonstrates the isotherms for CO_2/CH_4 binary mixture under different moisture contents. It can be noted that compared with dry shale organic nanopore, the adsorption capacity of CO_2 drops from ~14 mmol cm^{-3} to ~8 mmol cm^{-3} at the moisture content of 2.4 wt%. It can be attributed to the competitive adsorption occurred between H_2O molecules and CO_2/CH_4 mixture in shale nanopores. The H_2O molecules, which could be potentially adsorbed by CO_2/CH_4 in the dry state, adsorb to shale organic matter.

Fig. 14 presents the adsorption selectivity of CO_2/CH_4 as a function of moisture contents. It can be seen that compared with the nanopore in dry condition, moisture content would lower the selectivity of CO_2/CH_4 at all pressure conditions. The influences are different at low and high moisture contents. Specifically, the selectivity increases with the increasing moisture content at low moisture condition. However, an opposite trend has been found at high moisture condition, *i.e.*, >1.2 wt% in the present study. It is due to the tendency of selectivity is more determined by the decrease of CH_4 adsorption capacity at
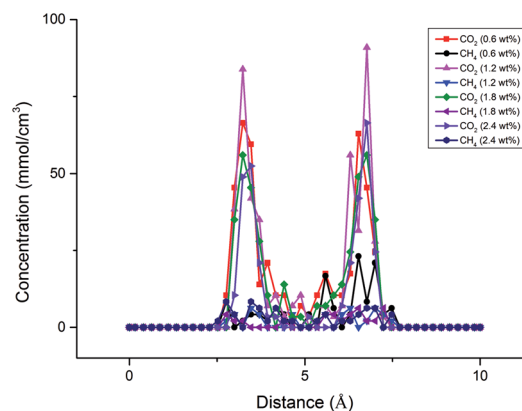

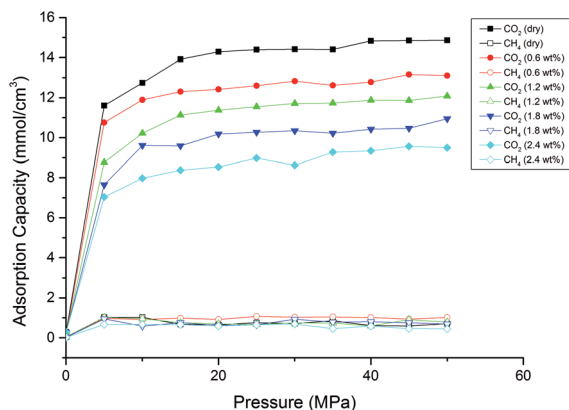Fig. 12 Concentration profile of CO_2/CH_4 binary mixture adsorption in the organic shale nanopore.

Fig. 13 Adsorption isotherms of CO_2/CH_4 binary mixture at different moisture contents.
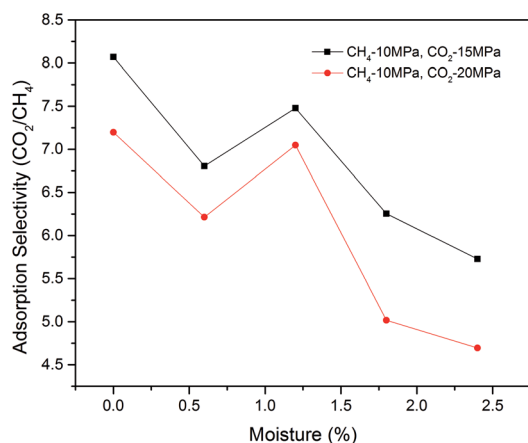

Fig. 14 Adsorption selectivity of CO_2/CH_4 in shale organic nanopore as a function of moisture contents at different pressures.

low moisture, which causes an increase of selectivity when the moisture is less than 1.2 wt%. A further increment of moisture content leads to a more notable decrease in the adsorption capacity of CO_2 than that of CH_4, causing a decrease in the adsorption selectivity of CO_2/CH_4. It is also observed that an increase of CO_2 injection pressure would decrease the selectivity. These findings would be useful for formulating the plans on enhancing shale gas recovery and CO_2 sequestration efficiency in CS-EGR project.

Conclusions

In this work, the competitive adsorption properties of CO_2/CH_4 binary mixture in shale organic nanopores were investigated by using a series of GCMC simulations. The effects of temperature, pressure, pore size and moisture content on CO_2/CH_4 competitive adsorption behaviours have been discussed in detail. Major conclusions are summarized as follows.

(1) The results show that CO_2 is preferentially adsorbed over CH_4 in the silt organic nanopore of shale formations. A lower temperature is favourable for both the adsorption capacity and selectivity of CO_2/CH_4 binary mixture.

(2) The increasing CO_2 injection pressure leads to an increase of adsorption capacity but a decline of selectivity. Therefore, an appropriate CO_2 injection pressure should be chosen to take into account the adsorption capacity and selectivity.

(3) Except extremely small pore size ($\sim$1 nm), the increase of pore size causes a decline of selectivity of CO_2/CH_4 binary mixture in shale organic nanopores. The optimum selectivity has been observed at the pore size of 1.5–2 nm.

(4) Compared with the dry state of shale organic matter, the presence of moisture content decreases the adsorption capacity of CO_2 and CH_4. The effect of moisture is more remarkable on CO_2 than that on CH_4. A fluctuation has been observed in selectivity with the increasing moisture content. Based on the results in this work, different strategies could be developed depending their real-time conditions of shale reservoirs in CS-EGR project.

Conflicts of interest

There are no conflicts to declare.

Acknowledgements

References

1 Y. Yang, L. Wang, Y. Fang and C. Mou, *Renewable Sustainable Energy Rev.*, 2016, **76**, 1465–1478.
2 L. Wang, S. Wang, R. Zhang, C. Wang, Y. Xiong, X. Zheng, S. Li, K. Jin and Z. Rui, *J. Nat. Gas Sci. Eng.*, 2017, **37**, 560–578.
3 M. Guo, X. Lu, C. P. Nielsen, M. B. McElroy, W. Shi, Y. Chen and Y. Xu, *Renewable Sustainable Energy Rev.*, 2016, **66**, 742–750.
4 G. A. Kahrilas, J. Blotevogel, P. S. Stewart and T. Borch, *Environ. Sci. Technol.*, 2015, **49**, 16–32.
5 A. Vengosh, R. B. Jackson, N. Warner, T. H. Darrah and A. Kondash, *Environ. Sci. Technol.*, 2014, **48**, 8334–8348.
6 R. Xu, R. Li, J. Ma, D. He and P. Jiang, *Acc. Chem. Res.*, 2017, **50**, 2056–2066.
7 Y. Zhang, T. Li, B. Chen, M. Nishio and Y. Song, *J. Chem. Eng. Data*, 2016, **61**, 873–880.
8 M. Bui, C. S. Adjiman, A. Bardow, E. J. Anthony, A. Boston, S. Brown, P. S. Fennell, S. Fuss, A. Galindo, L. A. Hackett, J. P. Hallett, H. J. Herzog, G. Jackson, J. Kemper, S. Krevor, G. C. Maitland, M. Matuszewski, I. S. Metcalfe, C. Petit, G. Puxty, J. Reimer, D. M. Reiner, E. S. Rubin, S. A. Scott, N. Shah, B. Smit, J. P. M. Trusler, P. Webley, J. Wilcox and N. Mac Dowell, *Energy Environ. Sci.*, 2018, **11**, 1062–1176.
9 C. Chen, Z. Chai, W. Shen, W. Li and Y. Song, *Energy Fuels*, 2017, **31**, 7317–7324.

10 J. B. Curtis, *AAPG Bull.*, 2002, **86**, 1921–1938.

11 C. Qin, Y. Jiang, Y. Luo, X. Xian, H. Liu and Y. Li, *Energy Fuels*, 2017, **31**, 493–503.

12 L. Huang, Z. Ning, Q. Wang, W. Zhang, Z. Cheng, X. Wu and H. Qin, *Appl. Energy*, 2018, **210**, 28–43.

13 T. H. Kim, J. Cho and K. S. Lee, *Appl. Energy*, 2017, **190**, 1195–1206.

14 L. Chen, Q. Kang, R. Pawar, Y.-L. He and W.-Q. Tao, *Fuel*, 2015, **158**, 650–658.

15 R. Xu, K. Zeng, C. Zhang and P. Jiang, *Appl. Therm. Eng.*, 2016, **115**, 1306–1314.

16 B. Yan, L. Mi, Y. Wang, H. Tang, C. An and J. E. Killough, *J. Pet. Sci. Eng.*, 2018, **160**, 498–509.

17 P. Weniger, W. Kalkreuth, A. Busch and B. M. Krooss, *Int. J. Coal Geol.*, 2010, **84**, 190–205.

18 S. Duan, M. Gu, X. Du and X. Xian, *Energy Fuels*, 2016, **30**, 2248–2256.

19 P. Charoensuppanimit, S. A. Mohammad and K. A. M. Gasem, *Energy Fuels*, 2016, **30**, 2309–2319.

20 T. F. T. Rexer, M. J. Benham, A. C. Aplin and K. M. Thomas, *Energy Fuels*, 2013, **27**, 3099–3109.

21 M. Gasparik, P. Bertier, Y. Gensterblum, A. Ghanizadeh, B. M. Krooss and R. Littke, *Int. J. Coal Geol.*, 2014, **123**, 34–51.

22 D. J. K. Ross and R. Marc Bustin, *Mar. Pet. Geol.*, 2009, **26**, 916–927.

23 Y. Jia, Y. Lu, D. Elsworth, Y. Fang and J. Tang, *J. Pet. Sci. Eng.*, 2018, **165**, 284–297.

24 X. Zhang, Y. Lu, J. Tang, Z. Zhou and Y. Liao, *Fuel*, 2017, **190**, 370–378.

25 B.-B. Wang, X.-D. Wang, W.-M. Yan and T.-H. Wang, *Langmuir*, 2015, **31**, 7457–7462.

26 S. Wang, Q. Feng, M. Zha, F. Javadpour and Q. Hu, *Energy Fuels*, 2018, **32**, 169–180.

27 B. Liu, C. Qi, T. Mai, J. Zhang, K. Zhan, Z. Zhang and J. He, *J. Nat. Gas Sci. Eng.*, 2018, **53**, 329–336.

28 H. Zhang, X. Zeng, Z. Zhao, Z. Zhai and D. Cao, *J. Nat. Gas Sci. Eng.*, 2017, **39**, 82–89.

29 M. Pathak, H. Huang, P. Meakin and M. Deo, *J. Nat. Gas Sci. Eng.*, 2018, **51**, 1–8.

30 K. Lin, Q. Yuan and Y.-P. Zhao, *Comput. Mater. Sci.*, 2017, **133**, 99–107.

31 H. Yu, J. Fan, J. Chen, Y. Zhu and H. Wu, *Int. J. Heat Mass Transfer*, 2018, **123**, 657–667.

32 J. Xiong, K. Liu, X. Liu, L. Liang and Q. Zeng, *RSC Adv.*, 2016, **6**, 110808–110819.

33 H. Sun, W. Sun, H. Zhao, Y. Sun, D. Zhang, X. Qi and Y. Li, *RSC Adv.*, 2016, **6**, 32770–32778.

34 T. Zhao, X. Li, Z. Ning, H. Zhao and M. Li, *J. Pet. Sci. Eng.*, 2018, **161**, 302–310.

35 B. Zhang, J. Kang and T. Kang, *Appl. Surf. Sci.*, 2018, **439**, 792–800.

36 M. Firouzi, E. C. Rupp, C. W. Liu and J. Wilcox, *Int. J. Coal Geol.*, 2014, **121**, 123–128.

37 H. Sun, H. Zhao, N. Qi and Y. Li, *J. Phys. Chem. C*, 2017, **121**, 10233–10241.

38 J. Xiong, X. Liu, L. Liang and Q. Zeng, *Energy Fuels*, 2017, **31**, 1489–1501.

39 P. M. Mathias and T. W. Copeman, *Fluid Phase Equilib.*, 1983, **13**, 91–108.

40 J. Xiong, X. Liu, L. Liang and Q. Zeng, *Fuel*, 2017, **200**, 299–315.

41 I. Langmuir, *J. Am. Chem. Soc.*, 1918, **40**, 1361–1403.

42 L. Huang, Z. Ning, Q. Wang, R. Qi, Y. Zeng, H. Qin, H. Ye and W. Zhang, *Fuel*, 2018, **211**, 159–172.

43 C. B. Pradip Chowdhury and S. Gumma, *J. Phys. Chem. C*, 2009, **113**, 6616–6621.

44 X. Xu, X. Zhao, L. Sun and X. Liu, *J. Nat. Gas Chem.*, 2008, **17**, 391–396.

45 F. Yang, Z. Ning, R. Zhang, H. Zhao and B. M. Krooss, *Int. J. Coal Geol.*, 2015, **146**, 104–117.